VNUHCM Journal of Science and Technology Development 2026, 29(2):4120-4135

Open Access Full Text Article

Research Article

Immobilization of Lewis acidic ionic liquid on layered double hydroxide and catalytic application in the synthesis of pyrido[1,2-*a*]pyrimidinone in solvent-free conditions

The Thai Nguyen[1,2,3], Thao Thanh Pham[1,2], Anh Thi Tram Tu[2,4], Phuong Hoang Tran[1,2,*]

ABSTRACT

In this study, a layered double hydroxide functionalized with an ionic liquid catalyst was synthesized and thoroughly characterized using advanced techniques, including FT-IR and Raman spectroscopy, XRD, TGA, SEM, and EDS. The results confirmed the formation and stability of the material, its layered structure, and the presence of the ionic liquid on its surface. The MgAl-LDH-IL material showed significant catalytic effectiveness and selectivity in the synthesis of pyrido[1,2-*a*]pyrimidinone. The reaction conditions for synthesizing pyrido[1,2-*a*]pyrimidinone were optimized, with the best results achieved under solvent-free conditions at 120 °C for 6 hours. Under these conditions, the reaction had a 65% yield with a 1:1 molar ratio of substrates. The solvent-free approach not only simplified the process but also reduced environmental and health risks, following the current trend toward green and sustainable chemistry. Furthermore, these reaction conditions were applied to synthesize four pyrido[1,2-*a*]pyrimidinones, with yields ranging from 13% to 65%. The physical properties of these derivatives, including color, state, and melting points, were determined, and their structural features were confirmed using ^{1}H NMR and ^{13}C NMR spectroscopy. The successful synthesis of these derivatives contributes to expanding the library of organic compounds with potential implementation in areas such as pharmaceuticals and material science. Overall, the combination of a heterogeneous catalyst and solvent-free conditions provides an economical, environmentally friendly, and scalable strategy for synthesizing biologically relevant heterocyclic compounds, in alignment with the principles of sustainable organic synthesis.

Key words: layered double hydroxide, ionic liquids, pyrido[1, 2-a]pyrimidinone, green catalyst

[1]*Department of Organic Chemistry, Faculty of Chemistry, University of Science, Ho Chi Minh City, Vietnam*

[2]*Vietnam National University, Ho Chi Minh City, Vietnam*

[3]*Faculty of Interdisciplinary Science, University of Science, Ho Chi Minh City, Vietnam*

[4]*Department of Magnetic and Biomedical Materials, Faculty of Materials Science and Technology, University of Science, Vietnam*

Correspondence

Phuong Hoang Tran, Department of Organic Chemistry, Faculty of Chemistry, University of Science, Ho Chi Minh City, Vietnam

Vietnam National University, Ho Chi Minh City, Vietnam

Email: thphuong@hcmus.edu.vn

History

- Received: 09-10-2025
- Revised: 24-01-2026
- Accepted: 24-02-2026
- Published Online: 24-06-2026

DOI : https://doi.org/10.32508/vnuhcmj-std.v29i2.4619

INTRODUCTION

Layered double hydroxides (LDHs), or hydrotalcite analogues, constitute a type of 2D anionic clay characterized by brucite-like cationic layers and compensating anions situated in the interlayer space. Their general formula is expressed as: [M1−x IIM^{x} III(OH)2]^{x}+ [Ax/n]$^{n-}$·mH2O, where M^{2+} (e.g., Mg^{2+}, Ni^{2+}, Cu^{2+}) and M3+ (e.g., Al^{3+}, Fe^{3+}) are metallic species carrying divalent and trivalent charges, and An− represents interlayer anions such as CO_3^{2-} or Cl^- [1]. LDH can be synthesized through various methods, such as co-precipitation, sol-gel, urea hydrolysis, and reconstruction techniques. Among them, the hydrothermal method is widely used due to its ability to produce highly crystalline and well-structured LDHs. In this method, metal salts and urea are dissolved in a solvent, and the mixture is treated under autogenous pressure in a sealed autoclave at 120-150 °C[2]. LDH materials, exhibiting high ion-exchange capacity, good thermal stability, and low toxicity, have been applied in various fields, including drug delivery, cell biology, polymer additives, and electrochemistry. Furthermore, these unique properties make them excellent candidates for applications in organic catalysis[3]. Last few years, numerous LDH-based catalytic systems have found applications in organic reactions. For instance, Rathee and co-workers have achieved a 94% yield of 1,4-dihydropyridines using Au/NiAlTi-LDH in ethanol under reflux[4]. Zhou and co-workers have used CuCoFe-LDH for a domino reaction in 1,4-dioxane at 80 °C, obtaining a 65% yield[5]. Hjazi and co-workers have used MgAl-LDH embedded in a hydrogel matrix to synthesize polyhydroquinolines at room temperature, reaching 90% yield[6]. Zhang and co-workers have synthesized indoles from 2-alkynylsulfonanilides using CuMgAl-LDH in ethanol, achieving 99% yield in 18 minutes[7].

During the last few years, numerous LDH-based catalytic systems have found applications in organic reactions. For instance, Rathee and co-workers have achieved a 94% yield of 1,4-dihydropyridines using Au/NiAlTi-LDH in ethanol under reflux[4]. Zhou and

Cite this article : Nguyen T T, Pham T T, Tu A T T, Tran P H. **Immobilization of Lewis acidic ionic liquid on layered double hydroxide and catalytic application in the synthesis of pyrido[1,2-*a*]pyrimidinone in solvent-free conditions**. *VNUHCMJ. Sci. Technol. Dev.* 2026; 29(2):4120-4135.

co-workers have used CuCoFe-LDH for a domino reaction in 1,4-dioxane at 80 °C, obtaining a 65% yield [5]. Hjazi and co-workers have used MgAl-LDH embedded in a hydrogel matrix to synthesize polyhydroquinolines at room temperature, reaching 90% yield (6). Zhang and co-workers have synthesized indoles from 2-alkynylsulfonanilides using CuMgAl-LDH in ethanol, achieving 99% yield in 18 minutes [7].

LDH-ILs, which integrate ionic liquids (ILs) into the LDH structure, have shown high efficiency and reusability in various organic transformations [8]. Hazrati Leilan and co-workers have used Fe_3O_4@CuMgAl-LDH/IMIL to synthesize tetrazole derivatives in DMF under reflux, yielding 96% [9]. Moradi and co-workers have synthesized 2,4,5-trisubstituted imidazoles in ethanol using MgAl-CO_3-LDH@Asn, achieving 98% yield [10]. Ghanbari and co-workers have performed a Biginelli-type reaction using MgAl-LDH@Melamine-PMA as the catalyst, reaching 95% yield [11]. Esfandiary and co-workers have obtained quinoline derivatives with 95% yield using γ-Fe_2O_3@Cu-LDH@Cysteine-Pd in choline azide [12].

Pyrido[1,2-*a*]pyrimidinone is a nitrogen-rich bicyclic heterocycle characterized by the fusion of a pyridine ring and a pyrimidinone ring, with the molecular formula $C_8H_6N_2O$. This fused scaffold forms a stable aromatic system commonly found in bioactive molecules. As a result, derivatives of pyrido[1,2-*a*]pyrimidinone have been shown to exhibit diverse pharmacological effects, such as antidepressant, antiallergic, and anticancer activities, making it a valuable core in medicinal chemistry [13]. Due to these promising bioactivities, considerable research has focused on developing efficient synthetic methods for pyrido[1,2-*a*]pyrimidinone derivatives. Pavithra and co-workers have synthesized 2*H*-pyrido[1,2-*a*]pyrimidin-2-ones from 2-aminopyridine and ethyl acetoacetate using sulfur under solvent-free conditions, with yields ranging from 54% to 97% (13). Alanine and co-workers have synthesized 4-methyl-2*H*-pyrido[1,2-*a*]pyrimidin-2-ones from *N*-(pyridin-2-yl)but-2-ynamide in DMSO, yielding 19%–99% [14]. Roslan and co-workers have synthesized 4*H*-pyrido[1,2-*a*]pyrimidin-4-ones from 2-aminopyridine and β-oxoester under solvent-free conditions using $BiCl_3$, with yields of 65%–99% [15]. Yan and co-workers have synthesized alkyl 4-oxo-4*H*-pyrido[1,2-*a*]pyrimidine-2-carboxylates from 2-aminopyridine and dialkyl acetylenedicarboxylates in water without a catalyst, with yields of 15%–97% [16]. Gaube and co-workers have synthesized 2-hydroxy-4*H*-pyrido[1,2-*a*]pyrimidin-4-ones from 2-aminopyridine and diethyl malonate under solvent-free conditions in N_2 atmosphere, with yields of 26%–56% [17].

The above synthetic methods for pyrido[1,2-*a*]pyrimidinone derivatives have limitations, including the use of non-green reagents/solvent/catalyst (such as sulfur, $BiCl_3$, or DMSO), and the need for an inert atmosphere. Many approaches also show poor substrate generality and require conditions that complicate purification or limit scalability. Hence, we developed a synthetic method of pyrido[1,2-*a*]pyrimidinone using the MgAl-LDH@$(CH_2)_3$DABCO@$Ni(OAc)_2$ catalyst.

MATERIALS AND METHODS

Materials

2-Aminopyridine (purity 98.0%), 2-amino-4-picoline (purity 98.0%), 2-aminobenzimidazole (purity 97.0%), ethyl acetoacetate (purity 99.0%), diethyl malonate (purity 99.0%), nickel(II) acetate tetrahydrate (purity 98.0%), nickel(II) chloride hexahydrate (purity 99.0%), copper(II) chloride (purity 97.0%), and cobalt(II) chloride hexahydrate (purity 97.0%), and triethylamine (purity 99.0%) were purchased from Sigma-Aldrich. Magnesium sulfate (purity 97.0%), aluminum nitrate (purity 97.0%), urea (purity 97.0%), toluene (purity 99.0%), and acetone (purity 99.5%) were purchased from Xilong. 3-Chloropropyltriethoxysilane (purity 99.4%) was purchased from Leyan.

Catalytic material preparation process

The preparation procedure of MgAl-LDH@$(CH_2)_3$DABCO@$Ni(OAc)_2$ required the four steps shown in Figure 1.

Synthesis of MgAl-LDH Support (A1): A mixture of $MgSO_4{\cdot}7H_2O$ (4.9 g), $Al(NO_3)_3{\cdot}9H_2O$ (3.7 g), and urea (0.9 g) was prepared in the molar ratio 2:1:1.5. The solid compounds were dissolved in a 9:1 (v/v) methanol/deionized water solution (90 mL MeOH:10 mL H_2O) under gentle stirring until complete dissolution. The solution was placed in a Teflon-lined autoclave and subjected to hydrothermal treatment at 150 °C for 12 hours. The solid was vacuum-filtered, rinsed with 100 mL of deionized water, and dried at 60 °C to achieve constant weight, yielding MgAl-LDH (A1) [2].

Grafting of 3-chloropropyltriethoxysilane onto MgAl-LDH (A2): MgAl-LDH (A1) (4.0 g) and 3-chloropropyltriethoxysilane (4.0 g) were introduced into a 100 mL round-bottom flask, followed by triethylamine (1.5 mL) and toluene (40 mL). The mixture was refluxed for 24 hours. After completion,

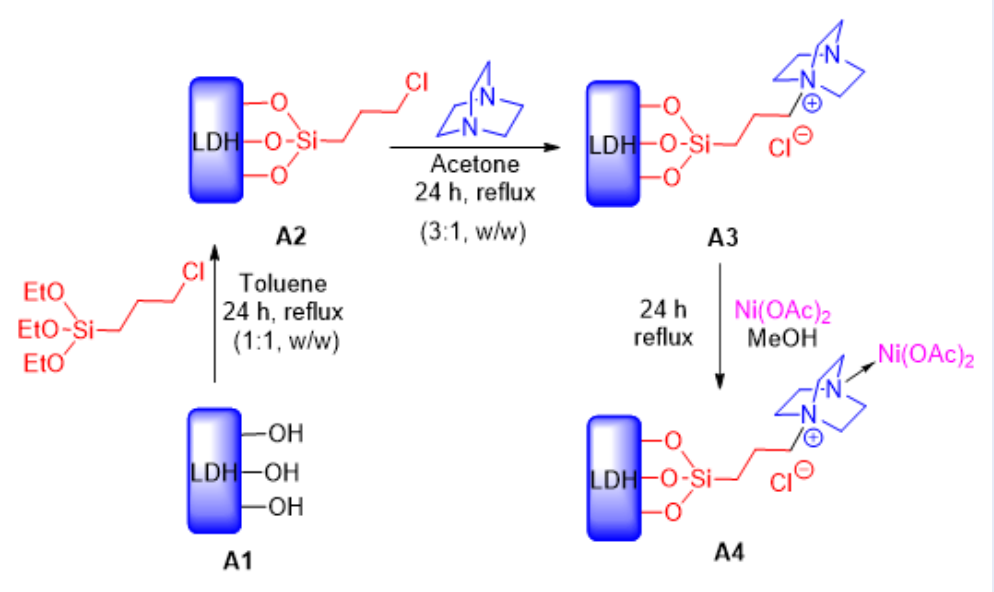

Figure 1: Preparation procedure of MgAl-LDH@$(CH_2)_3$DABCO@$Ni(OAc)_2$ material [Source: Authors']

the solid product was isolated by filtration, rinsed with acetone in five 20-mL portions, and dried at 60 °C under ambient conditions for 10 hours to produce material A2 [18].

Immobilization of DABCO on MgAl-LDH (A3): A2 (3.0 g) and DABCO (1.0 g) were introduced into a 100-mL round-bottom flask filled with 40 mL of acetone. The mixture was then heated under reflux for 24 hours. After the reaction, the solid product was collected by filtration, rinsed with acetone (5 × 20 mL), and dried at 60 °C for 10 hours, yielding the DABCO-functionalized LDH (A3) [18].

Incorporation of nickel into MgAl-LDH support (A4): A3 (3.0 g) and nickel(II) acetate (3.0 g) were dispersed in methanol (40 mL) and refluxed for 24 hours. Upon completion of the reaction, the catalyst was recovered using filter paper. The recovered solid was thoroughly washed with acetone (3 × 5 mL) to remove residual organics and then dried at 80 °C for 6 hours. The dried catalyst was then reused directly in subsequent reaction cycles under identical conditions to evaluate its recyclability and stability [18]. The formation of the material was confirmed using FT-IR spectroscopy, Raman spectroscopy, TGA, SEM, and EDS.

Preparation of pyrido[1,2-a]pyrimidinone derivatives

A mixture of 2-aminopyridine (1 mmol, 94.1 mg), ethyl acetoacetate (1.5 mmol, 195.2 mg), and 12 mol% of catalyst A4 (50.0 mg) was added to a 25-mL round-bottom flask. The reaction mixture was then heated and stirred at 120 °C for 6 hours (Figure 2). After the reaction was complete (determined by thin-layer chromatography), the mixture was diluted with 5 mL of acetone. The catalyst was then filtered and rinsed with acetone (3 × 5 mL). The solution was subsequently evaporated and purified by silica gel column chromatography using a hexane:acetone (9:1) eluent, yielding the pure product. The structure of the product was verified using ^1H and ^{13}C NMR spectroscopy. The recovered catalyst was washed thoroughly with acetone and methanol, then dried. After combining the material obtained from these separate reactions, the recovered catalyst was reused for the recycling experiments.

RESULTS AND DISCUSSION

Characterization of MgAl-LDH@$(CH_2)_3$DABCO@$Ni(OAc)_2$

The synthesis of IL-modified LDH materials was performed in four stages. First, material A1 was synthesized from $MgSO_4{\cdot}7H_2O$ and $Al(NO_3)_3{\cdot}9H_2O$ via the hydrothermal method. During this process, the mixture was heated to a high temperature, promoting the hydrolysis of urea, releasing ammonium carbonate, and increasing the pH of the solution. The mildly alkaline environment formed during the reaction facilitated the co-precipitation of Mg^{2+} and Al^{3+} cations along with anions, leading to the formation

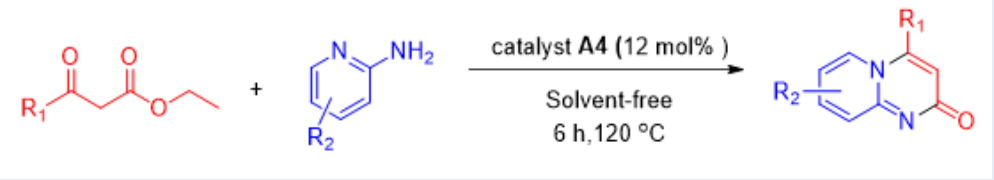

Figure 2: Synthesis of pyrido[1,2-*a*]pyrimidinones using MgAl-LDH@$(CH_2)_3$DABCO@Ni$(OAc)_2$catalyst [Source: Authors']

of the layered double hydroxide structure (MgAl-LDH). (3-Chloropropyl)triethoxysilane was used as a linker between the IL and the MgAl-LDH. The reaction between (3-chloropropyl)triethoxysilane and LDH proceeded via hydrolysis and condensation, with hydroxyl (-OH) groups on the LDH surface and the ethoxy (-OEt) groups of (3-chloropropyl)triethoxysilane forming -O-Si-CH_2- linkages, resulting in material A2. Next, DABCO reacted with A2 via a nucleophilic substitution reaction between the nitrogen atom of DABCO and the carbon atom directly bonded to the chlorine in (3-chloropropyl)triethoxysilane to produce A3. Finally, material A4 was formed by the complexation of A3 with nickel(II) acetate.

To determine the formation of bonds in the synthesized catalytic material, FT-IR spectroscopy was performed, and the resulting spectra are shown in Figure 3. The peaks at 600, 670, and 1070 cm^{-1} were characteristic of vibrations corresponding to M–O, M–OH, and O–M–O bonds derived from metal cations in the LDH structure. The broad absorption band at 3525 cm^{-1} corresponded to the stretching vibration of hydroxyl (–OH) groups on the surface of the hydroxide layer. Additionally, the absorption band at 1635 cm^{-1} was attributed to the bending vibration of H_2O molecules. The presence of interlayer anions was also indicated by the absorption signal at 1435 cm^{-1}, which corresponded to the stretching vibration of nitrate anions (NO_3^-)[19]. After surface functionalization with (3-chloropropyl)triethoxysilane, the FT-IR spectrum of catalyst A2 (Figure 3b) showed a new absorption band at 2980 cm^{-1}, assigned to the stretching vibration of H-Csp^3 bonds[18,20]. The FT-IR spectrum of catalyst A3 (Figure 3c) exhibits an additional absorption band at 1555 cm^{-1} of the C–N stretching vibrations, which confirms the successful modification of the material with DABCOium IL[18,21].

In the Raman spectrum of the MgAl-LDH-IL material (Figure 4), the signals at approximately 500 and 650 cm^{-1} were characteristic of M–O and M–OH bonds from metal cations (Mg, Al, and Ni) within the LDH layers[19,22]. The signal at 3600 cm^{-1} corresponded to the stretching vibration of hydroxyl (–OH) groups on the material surface. Additionally, the signal at 1050 cm^{-1} was attributed to the vibration of the interlayer nitrate anions (NO_3^-)[19].

The XRD pattern (Figure 5) shows characteristic diffraction peaks of the LDH structure at 2θ of 12°, 24°, 35°, 40°, 47°, 61°, and 62°, corresponding to the (003), (006), (009), (015), (018), (110), and (113) planes, respectively. In particular, the peaks at 2θ = 12° and 24°, assigned to the (003) and (006) planes, indicate interlayer distances of d_{003} = 7.43 Å and d_{006} = 3.74 Å, with a ratio of $d_{003} \approx 2 \times d_{006}$, confirming the structural regularity of the layered material. Several peaks show noticeable shifts relative to the standard values, suggesting that the two samples may not be structurally identical. These peak displacements may arise from partial distortion or disruption of the layered structure during synthesis or grinding, which can alter the lattice parameters. Overall, the XRD data of the LDH material matched the standard XRD pattern of MgAl-LDH (JCPDS No. 70-2151), confirming the development of a stable crystalline structure[2].

The TGA curve of MgAl-LDH@$(CH_2)_3$DABCO@Ni$(OAc)_2$ (Figure 6) shows three distinct weight loss stages. The first stage occurred below 200 °C, with approximately 10% weight loss assigned to the evaporation of solvents or water from within the LDH structure. From 200 to 430 °C, a 25% weight loss was observed, which corresponded to the decomposition of the IL, dehydroxylation, and the decomposition of the interlayer anions. Above 450 °C, 23% weight loss is detected due to the complete breakdown of the structure into metal oxides. These results indicated that the material was thermally stable below 200 °C, making it suitable for catalytic applications[23].

The SEM images (Figure 7) reveal the morphology and surface structure of MgAl-LDH@$(CH_2)_3$DABCO@Ni$(OAc)_2$ under different magnifications. At the lowest magnification (500×),

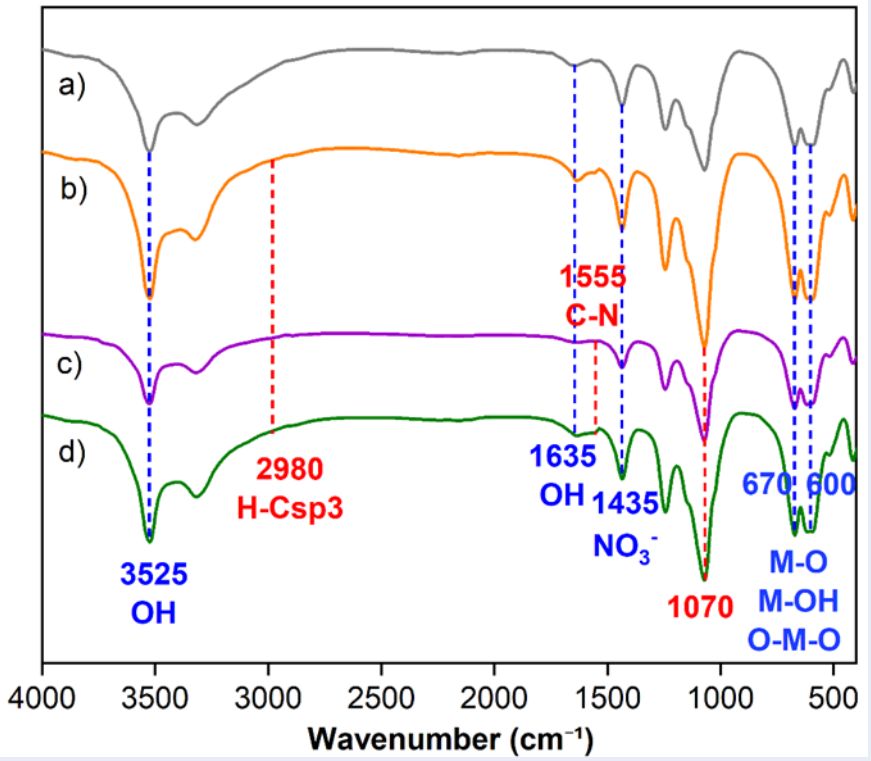

Figure 3: FT-IR spectra of a) MgAl-LDH (A1), b) MgAl-LDH@$(CH_2)_3$Cl (A2), c) MgAl-LDH@$(CH_2)_3$DABCO (A3), and d) MgAl-LDH@$(CH_2)_3$DABCO@Ni$(OAc)_2$(A4) [Source: Authors']

the surface of the IL-modified LDH appeared rough and heterogeneous. Upon modification with the viscous IL, the material tended to aggregate into larger clusters because the IL promoted particle agglomeration. The particle size of the LDH material ranged from 2 to 10 μm.

In addition, the elemental composition was analyzed using energy-dispersive X-ray spectroscopy (EDX). As shown in Figure 8 and Table 1 , the weight percentages of carbon, nitrogen, oxygen, magnesium, aluminum, silicon, sulfur, and nickel on the material surface were measured. The elemental distribution was further visualized using the mapping images in Figure 9.

Survey of the model reaction

The catalyst plays a crucial role in accelerating reaction rates and improving product yields. Therefore, the effect of various catalysts was investigated and evaluated. The reaction between 2-aminopyridine (1.0 mmol, 94.1 mg) and ethyl acetoacetate (1.5 mmol, 195.2 mg) was employed under solvent-free conditions at 120 °C for 6 hours. To determine the reaction yield, column chromatography was performed using a hexane:acetone (9:1, v/v) eluent. According to the results presented in Table 2, metal salt catalysts yielded only 0%–34% (entries 2–5). Specifically, $NiCl_2 \cdot H_2O$ and $CoCl_2 \cdot 6H_2O$ showed no catalytic activity (entries 3–4), while $CuCl_2$ led to 5% of the product (entry 5). The reaction can proceed under catalyst-free conditions because the starting materials possess sufficient intrinsic reactivity to undergo cyclization upon heating, although with low efficiency. However, when $NiCl_2$, $CoCl_2$, or $CuCl_2$ is added, these metal salts may coordinate with the substrates, inhibiting key steps of the reaction mechanism. Such coordination can reduce the nucleophilicity of the amine group or interfere with the condensation process, leading to no observable product [24].

In contrast, $Ni(OAc)_2 \cdot 4H_2O$ produced the target product with a yield of 34% (entry 2). The MgAl-LDH@$(CH_2)_3$DABCO@Ni$(OAc)_2$ catalyst achieved a higher yield of 56%. This improvement is attributed to the layered structure of the catalyst, which enhances catalytic activity. To further demonstrate the essential role of the IL-modified LDH catalyst in this transformation, the reaction was additionally performed without any catalytic

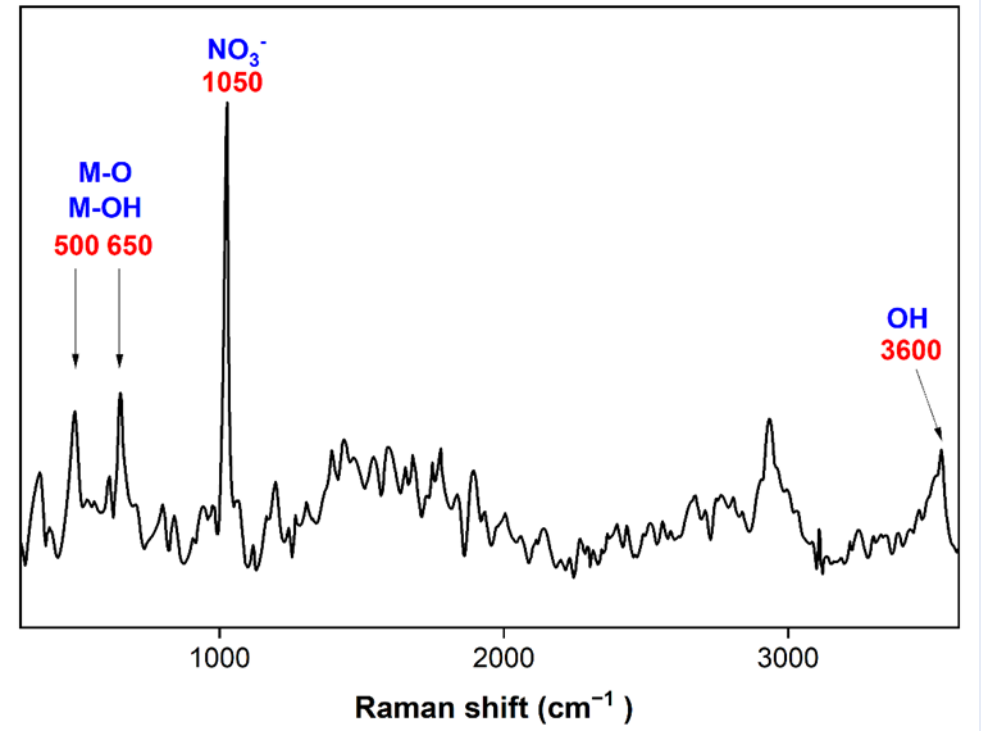

Figure 4: Raman spectrum of MgAl-LDH@$(CH_2)_3$DABCO@Ni$(OAc)_2$ [Source: Authors']

Table 1: EDS elemental distribution of MgAl-LDH@$(CH_2)_3$DABCO@Ni$(OAc)_2$ [Source: Authors']

Element	Weight (%)	Atomic (%)
C	10.73	17.89
N	2.29	3.27
O	40.74	51.11
Mg	1.01	0.83
Al	16.34	12.16
Si	1.68	1.20
S	14.61	9.15
Ni	12.28	4.22
Total	100.00	100.00

agent. The pyrido[1,2-*a*]pyrimidinone yield was only 14%, confirming the catalytic importance of MgAl-LDH@$(CH_2)_3$DABCO@Ni$(OAc)_2$.

Subsequently, the reaction time was optimized from 2 to 10 hours under the same reaction conditions (Figure 10). The results showed a yield increase when the reaction time increased from 2 to 6 hours (29%–56%). However, longer reaction times of 8 and 10 hours resulted in lower yields. The decrease in yield at extended reaction times may be attributed to partial evaporation of the liquid starting materials during prolonged heating.Therefore, 6 hours was the optimal reaction time.

The effect of temperature on the synthesis of pyrido[1,2-*a*]pyrimidinone was also investigated (Figure 11). A mixture of 2-aminopyridine (1.0 mmol), ethyl acetoacetate (1.5 mmol), and 12 mol% of MgAl-LDH@$(CH_2)_3$DABCO@Ni$(OAc)_2$ catalyst (50.0 mg) was heated under solvent-free conditions at various temperatures for 6 hours. The reaction

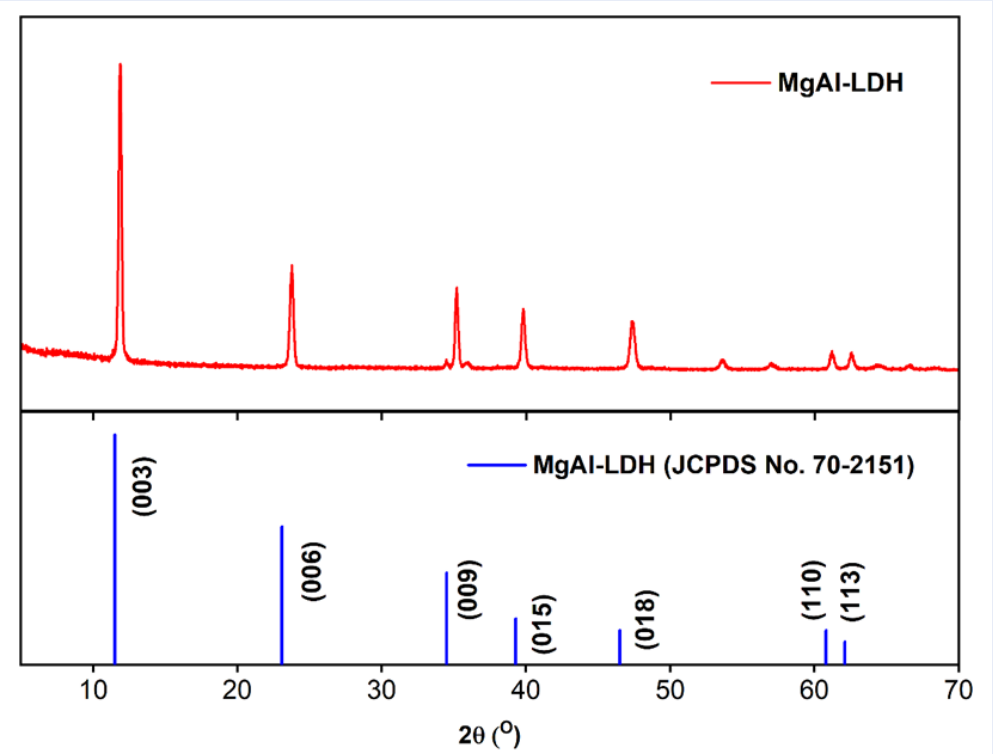

Figure 5: XRD pattern of MgAl-LDH@$(CH_2)_3$DABCO@$Ni(OAc)_2$ [Source: Authors']

Table 2: Influence of catalyst on the yield of 4-methyl-2*H*-pyrido[1,2-*a*]pyrimidin-2-one [Source: Authors']

No.	Catalyst	Yield (%)
1	Catalyst-free	14
2	$Ni(OAc)_2{\cdot}4H_2O$	34
3	$NiCl2{\cdot}6H_2O$	0
4	$CoCl_2{\cdot}6H_2O$	0
5	$CuCl_2$	5
6	MgAl-LDH (A1)	55
7	MgAl-LDH-IL (A4)	56

yields were low at 80 and 100 °C (14% and 24%, respectively), but increased significantly to 56% at 120 °C. When the temperature increased to 140 and 160 °C, the yields decreased to 37% and 45%, respectively. The yield fluctuation observed at temperatures above 120 °C is mainly attributed to the thermal decomposition of the intermediate species formed during the reaction. Under solvent-free conditions, evaporation of the liquid substrate at higher temperatures may also negatively affect reaction efficiency. Thus, 120 °C was determined to be the ideal temperature.

The effect of catalyst loading on the synthesis of pyrido[1,2-*a*]pyrimidinone was also investigated. The reaction between 2-aminopyridine (1.0 mmol) and ethyl acetoacetate (1.5 mmol) was conducted in the absence of solvent at 120 °C for 6 hours, with varying amounts of MgAl-LDH@$(CH_2)_3$DABCO@$Ni(OAc)_2$ catalyst (corresponding to 2–22 mol% Ni^{2+}, 10–90 mg). In the absence of a catalyst, the reaction gave a low yield of 14% (Table 2, entry 1). As shown in Figure 12, the yield gradually increased with catalyst loading from 2 to 12 mol% Ni, reaching 27%, 35%, and a maximum

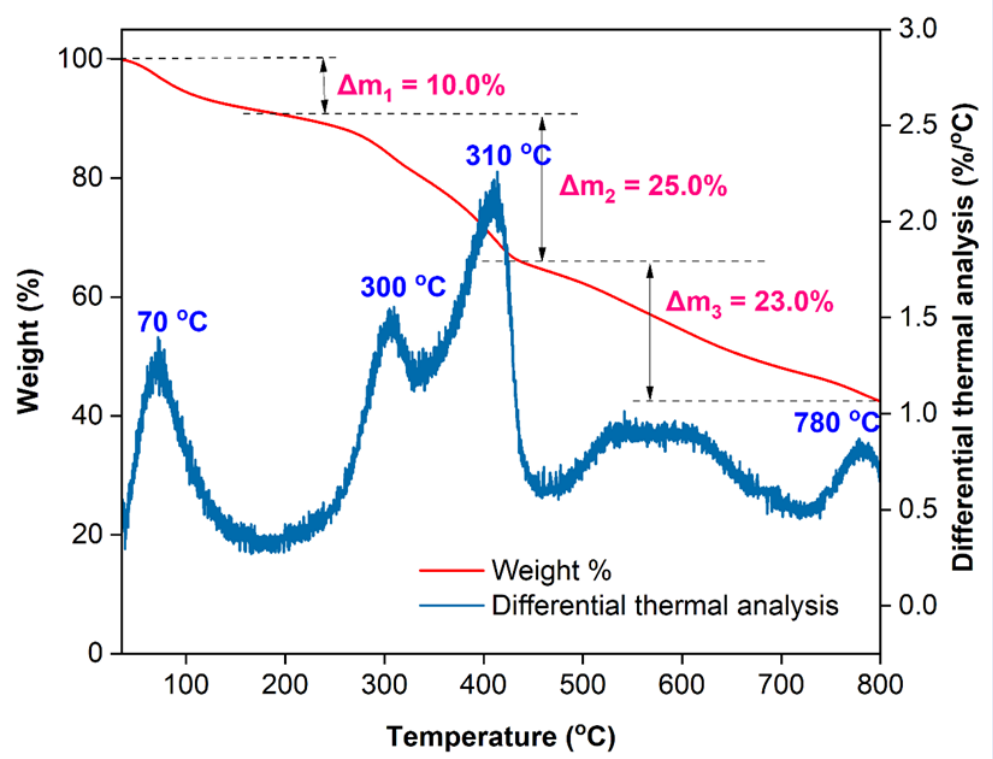

Figure 6: TGA of MgAl-LDH@$(CH_2)_3$DABCO@Ni$(OAc)_2$ [Source: Authors']

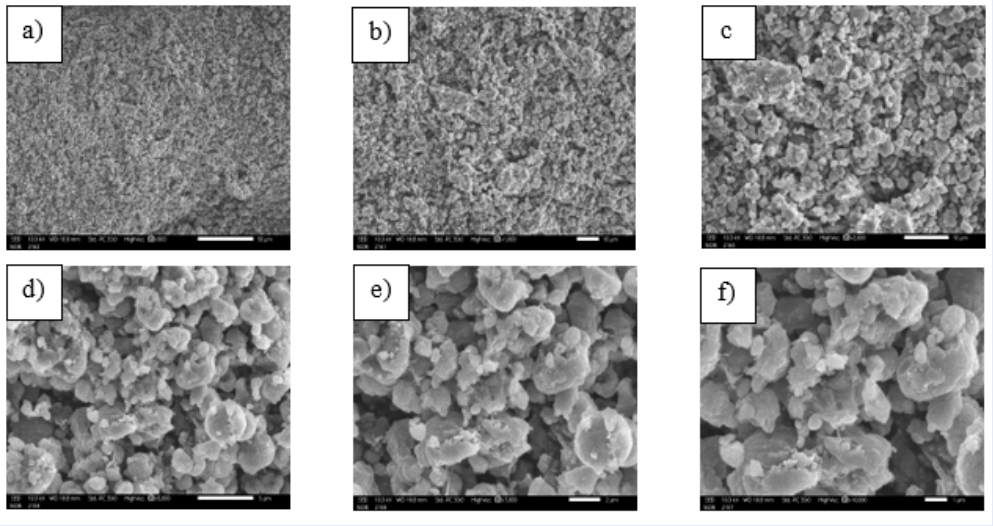

Figure 7: SEM images of MgAl-LDH@$(CH_2)_3$DABCO@Ni$(OAc)_2$ at a)500×, b) 1000×, c) 2000×, d) 5000×, e) 7000×, and f) 10000× magnification [Source: Authors']

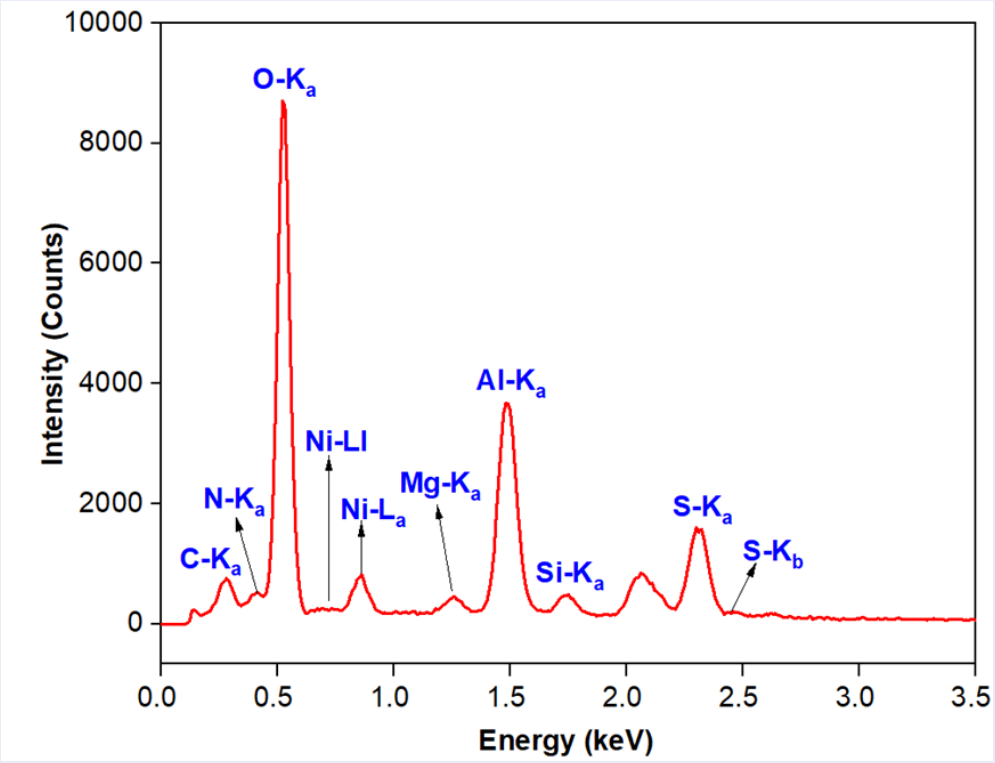

Figure 8: EDS of MgAl-LDH@$(CH_2)_3$DABCO@Ni$(OAc)_2$ [Source: Authors']

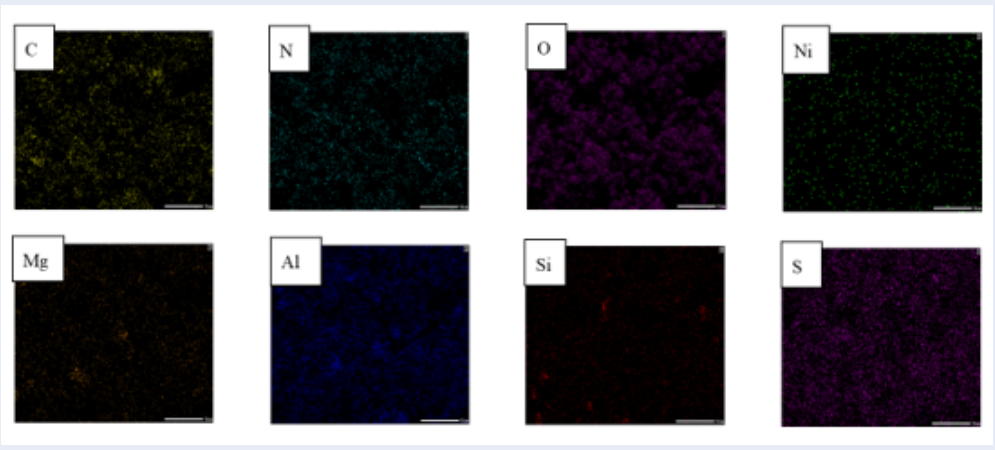

Figure 9: EDS maps of MgAl-LDH@$(CH_2)_3$DABCO@Ni$(OAc)_2$ [Source: Authors']

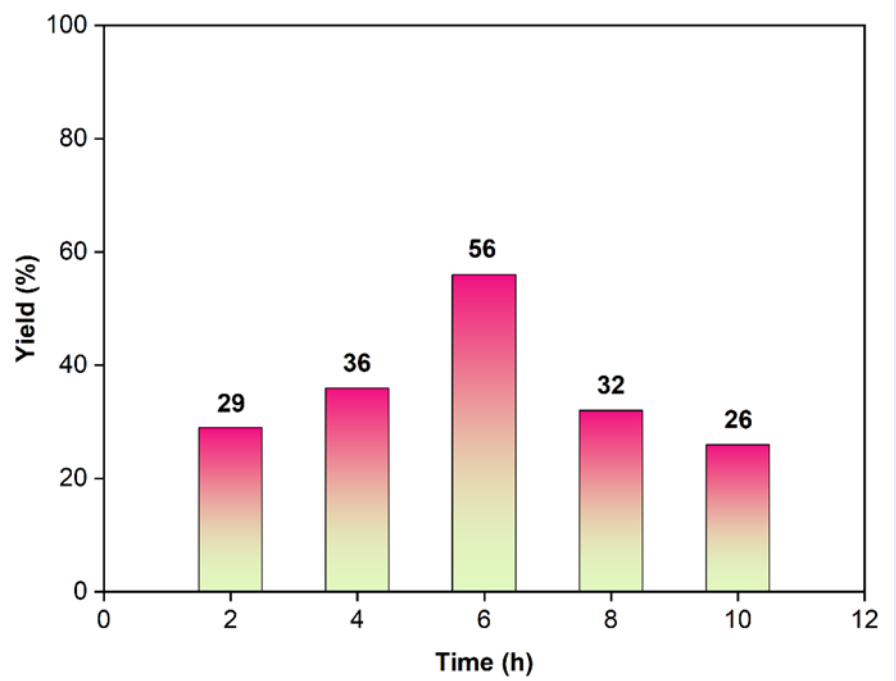

Figure 10: Influence of reaction time on yield of 4-methyl-2*H*-pyrido[1,2-*a*]pyrimidin-2-one [Source: Authors']

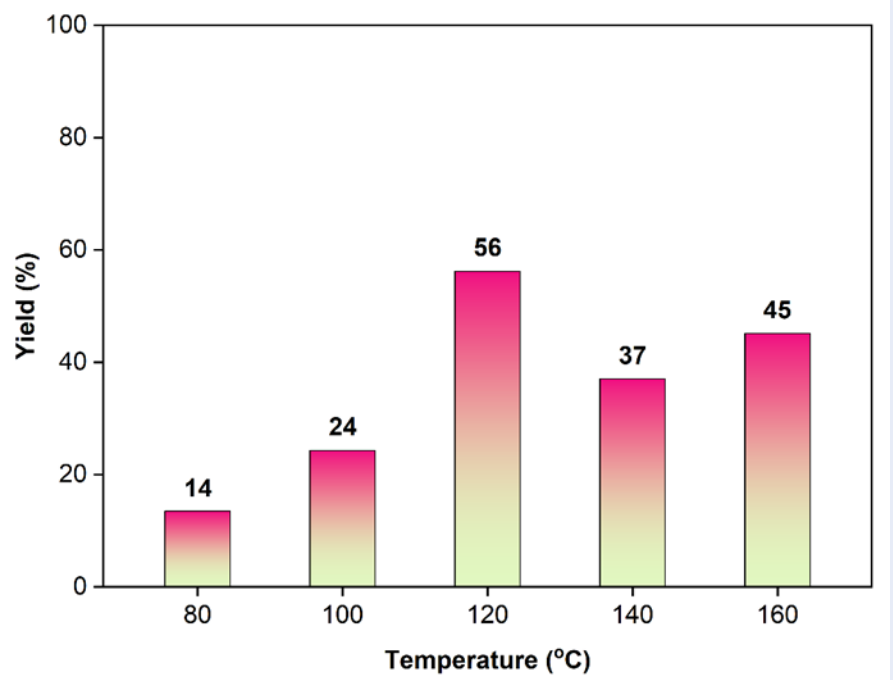

Figure 11: Influence of temperature on the yield of 4-methyl-2*H*-pyrido[1,2-*a*]pyrimidin-2-one [Source: Authors']

of 56%. The number of active catalytic sites directly influences the yield. When the catalyst loading is sufficient, there are enough active sites to promote the reaction efficiently. However, increasing the amount of catalyst (17 and 22 mol% Ni) decreased the reaction efficiency (49% and 31%, respectively). This decrease is attributed to particle agglomeration under solvent-free conditions, which blocked active sites on the solid catalyst and hindered the interaction between reactant molecules. Thus, the optimal catalyst loading was 12 mol% Ni^{2+} (50 mg).

Because MgAl-LDH@$(CH_2)_3$DABCO@Ni$(OAc)_2$ is a solid catalyst, the effect of various solvents was surveyed. The experiment was implemented at 120 °C for 6 hours using 2-aminopyridine (1.0 mmol), ethyl acetoacetate (1.5 mmol), and 12 mol% catalyst (50 mg). Some high-boiling solvents (above 120 °C) were selected. As shown in Figure 13, the reactions in all solvents resulted in lower yields compared to the solvent-free condition. The yields in toluene, sulfolane, , -dimethylformamide, and dimethyl sulfoxide were 28%, 38%, 23%, and 14%, respectively. Ethylene glycol produced only 5% of the target product. These data were lower than the 56% yield obtained under solvent-free conditions. Ethyl acetoacetate could dissolve 2-aminopyridine at 120 °C, allowing homogeneous mixing and efficient dispersion of the solid catalyst in the reaction mixture. Under solvent-free conditions, the reactants were in direct contact, resulting in a higher collision frequency and an increased reaction rate, ultimately enhancing the yield. In contrast, when a solvent was present, dilution reduced the effective reactant concentrations and their interactions, leading to lower yields. Therefore, the solvent-free condition was identified as optimal for this synthetic procedure.

Next, the effect of varying the molar ratios of reactants on the synthesis of pyrido[1,2-*a*]pyrimidinone was evaluated under solvent-free conditions at 120 °C for 6 hours with 12 mol% MgAl-LDH@$(CH_2)_3$DABCO@Ni$(OAc)_2$ catalyst. The molar ratios of 2-aminopyridine and ethyl acetoacetate were 0.8:1.0, 1.0:1.0, 1.0:1.2, and 1.0:1.5. The results in Table 3 show that product yield depended on the substrate ratio. At a 0.8:1.0 ratio, the yield was only 41%, indicating that a deficiency of ethyl acetoacetate reduced reaction efficiency. The maximum yield of 65% was achieved at a 1.0:1.0 molar ratio, suggesting that a balanced stoichiometry provides the best reaction efficiency. Increasing the ratio to 1.0:1.2 sharply decreased the yield (39%), while an increase to 1.0:1.5 improved the yield slightly to 56%. Therefore, the substrate ratio of 1.0:1.0 was the most effective for the synthesis of pyrido[1,2-*a*]pyrimidinone.

To determine the role of the MgAl-LDH@$(CH_2)_3$DABCO@Ni$(OAc)_2$ catalyst in the synthesis of pyrido[1,2-*a*]pyrimidinone, a leaching test was performed. The cyclization of 2-aminopyridine (1.0 mmol) and ethyl acetoacetate (1.5 mmol) was conducted under solvent-free conditions at 120 °C using 12 mol% of catalyst (50.0 mg). After 4 hours, the catalyst was filtered from the reaction mixture, and the reaction proceeded under the same conditions without the catalyst for an additional 2 hours. After the catalyst was removed, the reaction performance increased slightly from 36% to 39%. This indicated that no significant leaching of the active catalytic species into the reaction mixture occurred. In contrast, when the catalyst was retained throughout the 6-hour reaction time, the yield reached 56%. This demonstrates the necessity of the catalyst for achieving optimal efficiency in the synthesis of pyrido[1,2-*a*]pyrimidinone (Figure 14).

Synthesis of pyrido[1,2-*a*]pyrimidinone derivatives

To evaluate the applicability of this reaction to different substrates, various derivatives of 2-aminopyridine were also investigated. When 2-amino-4-picoline was used as the amine component, the reaction had a yield of 65% (Table 4, entry 2), higher than that obtained with unsubstituted 2-aminopyridine (Table 4, entry 1). This result suggests that the methyl substituent (-CH_3) on the pyridine ring had an electron-donating inductive effect, enhancing the nucleophilicity of the nitrogen lone pair and facilitating the nucleophilic addition step of the reaction. In addition, 2-aminobenzimidazole was found to participate in the cyclization with ethyl acetoacetate to provide product 3c at 24% yield (Table 4, entry 3). Furthermore, diethyl malonate was explored as a substrate in this conversion. The reaction between diethyl malonate and 2-aminopyridine afforded product 3d with 43% yield (Table 4, entry 4). Similarly, product 3e was obtained by cyclization of diethyl malonate with 2-amino-4-picoline in 13% yield (Table 4, entry 5). All pyrido[1,2-*a*]pyrimidinone derivatives were characterized by ^1H and ^{13}C NMR spectroscopy (Supporting Information).

The results of the current synthetic procedure are compared with those of previous methods in Table 5. Overall, prior methods for the synthesis of pyrido[1,2-*a*]pyrimidinone have demonstrated good to excellent yields across various reaction pathways,

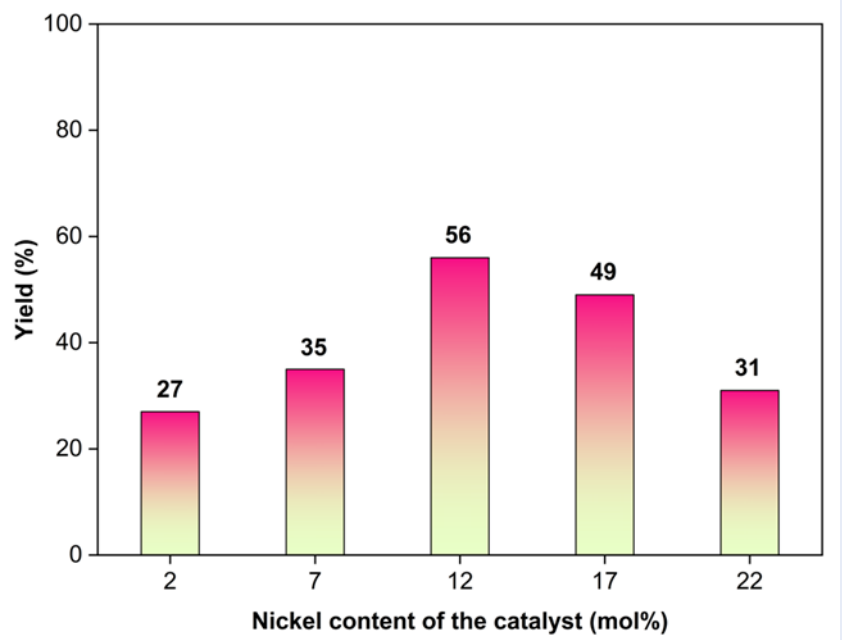

Figure 12: Influence of catalyst loading on the yield of 4-methyl-2*H*-pyrido[1,2-*a*]pyrimidin-2-one [Source: Authors']

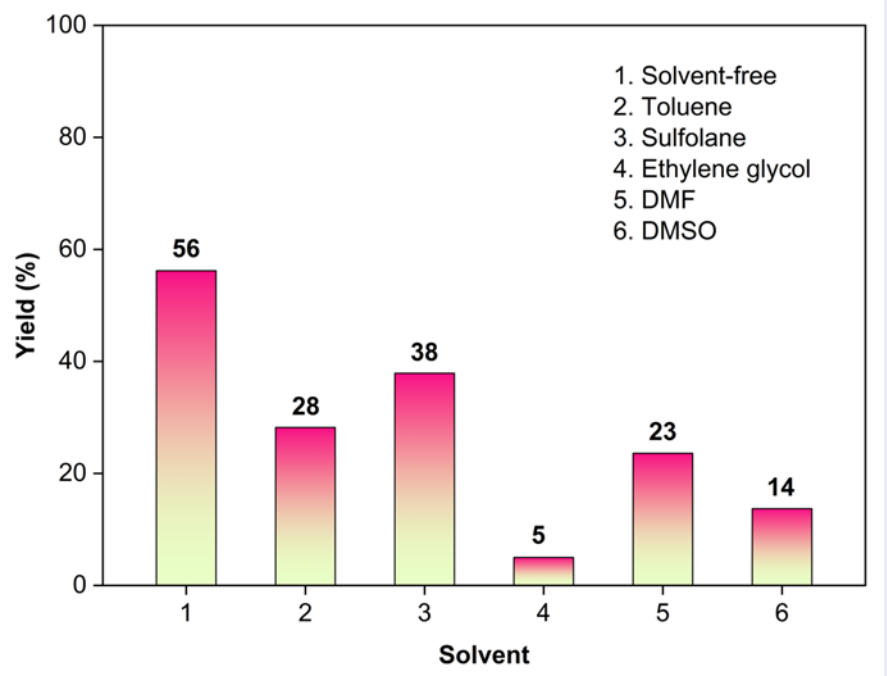

Figure 13: Influence of solvent on the yield of 4-methyl-2*H*-pyrido[1,2-*a*]pyrimidin-2-one [Source: Authors']

Table 3: Influence of substrate loading on the yield of 4-methyl-2*H*-pyrido[1,2-*a*]pyrimidin-2-one [Source: Authors']

No.	Substrate loading (2-aminopyridine:ethyl acetoacetate)	Yield (%)
1	0.8:1	41
2	1:1	65
3	1:1.2	39
4	1:1.5	56

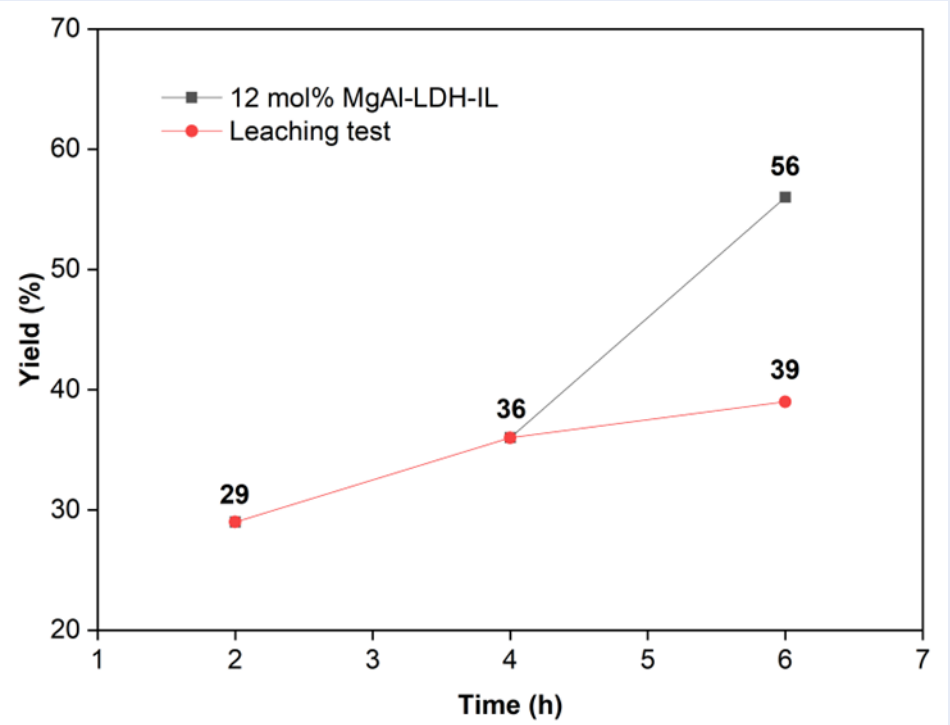

Figure 14: Leaching test results [Source: Authors']

including solvent-free systems, aqueous media, and diverse catalysts, with yields varying significantly depending on the substrate combinations and reaction strategies. In the present study, under IL-modified double-layer hydroxide catalyst and solvent-free conditions, this new method achieved high yields (13%–65%). The catalyst was easily recovered and reused, and solvent-free conditions helped minimize costs and negative environmental impacts, opening up prospects for large-scale development of this process.

Reaction mechanism

To gain insight into the mechanism of pyrido[1,2-*a*]pyrimidinone formation, several control experiments were conducted. In the absence of the MgAl-LDH@$(CH_2)_3$DABCO@Ni$(OAc)_2$ catalyst, the reaction yield was only 14% (Figure 15), indicating the essential function of the catalyst in promoting the conversion. The proposed pathway for the cyclization of 2-aminopyridine with ethyl acetoacetate is illustrated in Figure 15. At the initial stage, the carbonyl group of ethyl acetoacetate is activated by the Ni^{2+} species in the catalyst. The non-bonding pair of electrons on the amino group of 2-aminopyridine acts as a nucleophile and attacks the carbon atom of the ester carbonyl group, forming a zwitterionic tetrahedral intermediate A. Subsequently, an ethanol molecule is eliminated, leading to the formation of intermediate C via intermediate B. In the second stage, the lone pair of electrons on the nitrogen atom in the pyridine ring undergoes intramolecular nucleophilic attack on the

Table 4: Synthesis of pyrido[1,2-*a*]pyrimidinonederivatives [Source: Authors']

No.	Amine	β-dicarbonyl ester	Product	Yield[a] (%)
1	2-Aminopyridine	Ethyl acetoacetate	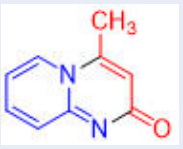 (3a)	56
2	2-Amino-4-picoline	Ethyl acetoacetate	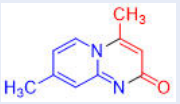 (3b)	65
3	2-Aminobenzimidazole	Ethyl acetoacetate	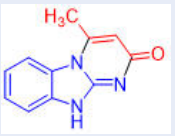 (3c)	24
4	2-Aminopyridine	Diethyl malonate	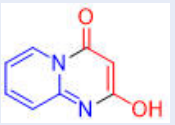 (3d)	43
5	2-Amino-4-picoline	Diethyl malonate	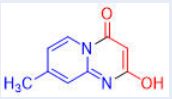 (3e)	13

[a]The isolated yield was determined by column chromatographyusing a hexane:acetone solvent system (9:1, v/v).

Table 5: Comparison of syntheses of pyrido[1,2-*a*]pyrimidinones [Source: Authors']

No.	Catalyst	Substrate	Reaction conditions	Yield (%)
1	Polyphosphoric acid	-(1,3-dioxobutyl)-2-amino pyridine	110 °C, 4 hour	52–72(25)
2	Sulfur	2-aminopyridine, ethyl acetoacetate	120 °C, 2 hour	54–97(13)
3		N-(pyridin-2-yl)but-2-ynamide	DMSO, 85 °C, 45 hour	19–99(14)
4		2-aminopyridine, methyl 2-(hydroxymethyl) acrylate	HFIP, 80 °C, 12 hour	52–95(26)
5		2-aminopyridine, diethyl malonate	N2, 230 °C, 3 hour	26–56(17)
6		2-aminopyridine, methyl acrylate	HFIP, 80 °C, 12-48 hour	70–98(27)
7	A4	2-aminopyridine, ethyl acetoacetate	120 °C, 6 hour	13–65

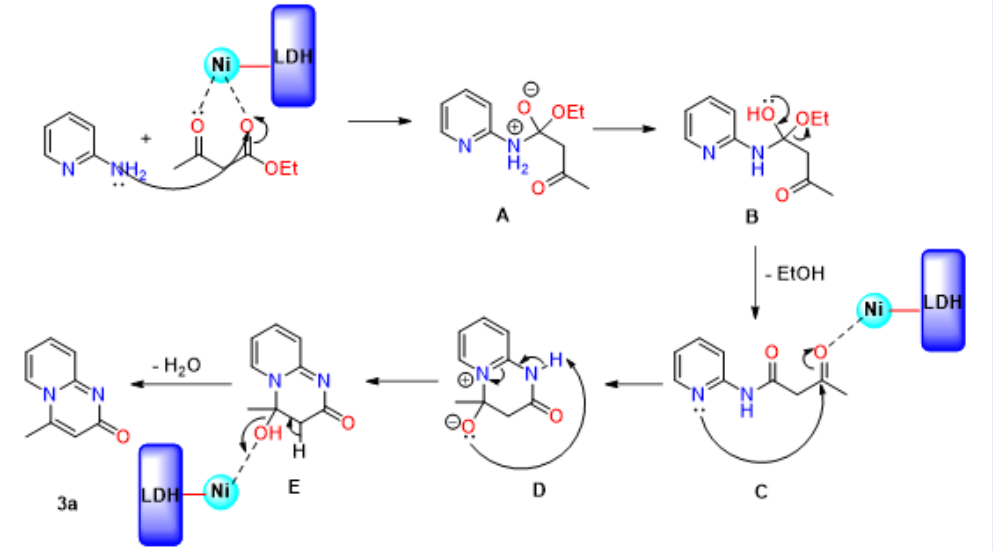

Figure 15: Reaction mechanism for synthesis of pyrido[1,2-*a*]pyrimidinone through the cyclization of 2-aminopyridine and ethyl acetoacetate

remaining activated carbonyl group, resulting in intermediate D. The proton transfer leads to the formation of intermediate E. Finally, dehydration of intermediate E yields the target product 3a.

CONCLUSIONS

In this study, MgAl-LDH@$(CH_2)_3$DABCO@Ni$(OAc)_2$ catalyst was synthesized and characterized using advanced techniques, confirming its layered structure and IL functionalization. The catalyst showed high activity in the solvent-free synthesis of pyrido[1,2-*a*]pyrimidinone at 120 °C for 6 hours using a 1:1 substrate ratio. The catalyst was easily recovered and reused without loss of performance. Five derivatives were also synthesized under the same conditions with yields of 13%–65%, and their structures were confirmed by NMR spectroscopy. This work presents a green, economical, and scalable method for synthesizing bioactive heterocycles.

LIST OF ABBREVIATIONS

DABCO: 1,4-diazabicyclo[2.2.2]octane
DMSO: Dimethyl sulfoxide
EDS: Energy-dispersive X-ray spectroscopy
FT-IR: Fourier-transform infrared spectroscopy
IL: Ionic liquid
LDH: Layered double hydroxide
NMR: Nuclear magnetic resonance
SEM: Scanning electron microscope
TGA: Thermal gravimetric analysis
XRD: X-Ray diffraction

ACKNOWLEDGEMENTS

This research is funded by Vietnam National Foundation for Science and Technology Development (NAFOSTED) under grant number 104.01-2023.29.

COMPETING INTERESTS

The authors declare that they have no competing interests.

AUTHORSHIP CONTRIBUTION STATEMENT

The Thai Nguyen: Conceptualization, Investigation, Methodology, Formal analysis, Writing – original draft, Validation. Thao Thanh Pham: Investigation, Methodology, Writing – original draft. Anh Thi Tram Tu: Method, Supervision. Phuong Hoang Tran: Funding, Writing – review & editing, Supervision.

REFERENCES

1. Li T, Miras HN, Song YF. Polyoxometalate (POM)-layered double hydroxides (LDH) composite materials: Design and catalytic applications. Catalysts. 2017;7(9):253.
2. Sarma GK, Rashid MH. Synthesis of Mg/Al layered double hydroxides for adsorptive removal of fluoride from water: A mechanistic and kinetic study. Journal of Chemical & Engineering Data. 2018;63(8):2957–2965.
3. Arrabito G, Bonasera A, Prestopino G, Orsini A, Mattoccia A, Martinelli E. Layered double hydroxides: A toolbox for chemistry and biology. Crystals. 2019;9(7):361.

4. Rathee G, Kohli S, Panchal S, Singh N, Awasthi A, Singh S. Fabrication of a gold-supported NiAlTi-layered double hydroxide nanocatalyst for organic transformations. ACS Omega. 2020;5(38):23967–23974.
5. Zhou W, Wang A, Kong Z, Tian X, Xia Z, Zhang Z. Construction of indoline-fused tetrahydroisoquinolines through a domino coupling reaction catalyzed by CuCoFe layered double hydroxide. Organic Letters. 2021;23(16):6321–6325.
6. Hjazi A. Fabrication of a novel magnetic nanostructure based on cellulose-gellan gum hydrogel, embedded with MgAl LDH as an efficient catalyst for the synthesis of polyhydroquinoline derivatives. International Journal of Biological Macromolecules. 2024;271:132547.
7. Zhang SY, Sun SG, Guo YS, Lu XF, Guo DS. An efficient synthesis of indoles via a CuMgAl-LDH-catalyzed cyclization of 2-alkynylsulfonanilides. Tetrahedron Letters. 2018;59(41):3719–3723.
8. Li T, Zhang W, Chen W, Miras HN, Song YF. Layered double hydroxide anchored ionic liquids as amphiphilic heterogeneous catalysts for the Knoevenagel condensation reaction. Dalton Transactions. 2018;47(9):3059–3067.
9. Leilan AH, Babazadeh M, Hekmati M, Ghasemi E. Application of modified copper-doped Fe3O4@CuMgAl-LDH nanoreactor with imidazolium ionic liquid as a reusable catalyst for synthesis of tetrazoles from aryl halides. Inorganic Chemistry Communications. 2023;155:111044.
10. Moradi S, Ardeshiri HH, Gholami A, Ghafuri H. Synthesis and characterization of new biocatalyst based on LDH functionalized with l-asparagine amino acid for the synthesis of trisubstituted derivatives of 2, 4, 5-(1H)-imidazoles. Heliyon. 2023;9(11):e22185.
11. Ghanbari N, Ghafuri H. Pyromellitic acid grafted to cross-linked LDH by dendritic units: An efficient and recyclable heterogeneous catalyst for green synthesis of 2,3-dihydro quinazoline and dihydropyrimidinones derivatives. Heliyon. 2023;9(11):e20978.
12. Esfandiary N, Bagheri S, Heydari A. Magnetic $γ$-Fe2O3@Cu-LDH intercalated with palladium cysteine: An efficient dual nano catalyst in tandem CN coupling and cyclization progress of synthesis quinolines. Applied Clay Science. 2020;198:105841.
13. Pavithra T, Devi ES, Nagarajan S, Sridharan V, Maheswari CU. Metal and solvent-free synthesis of 2H-pyrido[1,2-a]pyrimidin-2-ones catalyzed by elemental sulfur. European Journal of Organic Chemistry. 2019;2019(40):6884–6887.
14. Alanine TA, Galloway WRJD, Bartlett S, Ciardiello JJ, McGuire MC, Spring DR. Concise synthesis of rare pyrido[1,2-a]pyrimidin-2-ones and related nitrogen-rich bicyclic scaffolds with a ring-junction nitrogen. Organic & Biomolecular Chemistry. 2016;14(3):1031–1038.
15. Roslan II, Lim QX, Han A, Chuah GK, Jaenicke S. Solvent-free synthesis of 4H-Pyrido[1,2-a]pyrimidin-4-ones catalyzed by BiCl3: A green route to a privileged backbone. European Journal of Organic Chemistry. 2015;2015(11):2351–2355.
16. Yan H, Ma Y, Sun Y, Ma C, Wang Y, Ren X. Catalyst-free synthesis of alkyl 4-oxo-4H-pyrido[1,2-a]pyrimidine-2-carboxylate derivatives on water. Tetrahedron. 2014;70(17):2761–2765.
17. Gaube G, Mutter J, Leitch DC. A "neat" synthesis of substituted 2-hydroxy-pyrido[1,2-a]pyrimidin-4-ones. Canadian Journal of Chemistry. 2024;102(4):206–213.
18. Sobhani S, Pakdin-Parizi Z. Palladium-DABCO complex supported on $γ$-Fe2O3 magnetic nanoparticles: A new catalyst for C-C bond formation via Mizoroki-Heck cross-coupling reaction. Applied Catalysis A: General. 2014;479:112–120.
19. Iqbal MA, Secchi M, Iqbal MA, Montagna M, Zanella C, Fedel M. MgAl-LDH/graphene protective film: Insight into LDH-graphene interaction. Surface and Coatings Technology. 2020;401:126253.
20. Adam F, Osman H, Hello KM. The immobilization of 3-(chloropropyl)triethoxysilane onto silica by a simple one-pot synthesis. Journal of Colloid and Interface Science. 2009;331(1):143–147.
21. Nguyen TT, Nguyen TP, Tran LN, Huynh TTT, Nguyen NH, Nguyen LHT. DABCOnium ionic liquid-immobilized silica gel for solid phase extraction of phenoxyacetic acid herbicides in water samples. ChemistrySelect. 2022;7(46):e202203526.
22. Kim TH, Koo KY, Park CS, Jeong SU, Kim JE, Lee SH. Effect of Fe on calcined Ni(OH)2 anode in alkaline water electrolysis. Catalysts. 2023;13(3):496.
23. Li Y, Zhang Q, Zhou W, Huang Y, Han J. Study on the dispersion and lubrication properties of LDH in lubricating oil. Lubricants. 2023;11(3):147.
24. Haas KL, Franz KJ. Application of metal coordination chemistry to explore and manipulate cell biology. Chemical Reviews. 2009;109(10):4921–4960.